EVS26
Los Angeles, California, May 6-9, 2012

Analyzing Calendar Aging Data towards a Lifetime Prediction Model for Lithium-Ion Batteries

M. Ecker[1], J. B. Gerschler, J. Vogel, S. Käbitz, F. Hust, P. Dechent, D. U. Sauer
[1] *Madeleine Ecker (corresponding author) Institute for Power Electronics and Electrical Drives (ISEA), RWTH Aachen University, Jaegerstrasse 17-19, D-52066 Aachen, Germany, er@isea.rwth-aachen.de; (batteries@isea.rwth-aachen.de)*

Abstract

For a reliable integration of batteries into the vehicle, knowledge about battery behavior and especially the lifetime of the battery in the application is indispensible. This work aims at the development of a lifetime prediction approach based on an aging model for lithium-ion batteries. Extended accelerated lifetime tests are performed at different temperatures and states of charge (SOC) to investigate the impact of these conditions on the impedance rise and capacity loss. The results are used to find mathematical expressions describing the impact of storage time, temperature and voltage on aging, to build up a model coupling an impedance-based electric-thermal part with a semi-empirical (physically motivated) aging model. Based on these models different drive cycles, use patterns and management strategies can be analyzed with regard to their impact on the lifetime. This is an important tool for vehicle designers and for the implementation of business models. The strength of this paper is the good data basis and the detailed modeling approach.

Keywords: Lithium-ion, aging, lifetime prognosis, battery model, HEV

1. Introduction

Lifetime prediction for lithium-ion batteries under real operation is a key issue for a reliable integration of the battery into the vehicle and for warranty issues. As aging tests using real operation conditions are very time and cost intensive, accelerated aging tests are discussed to be a powerful method. To extrapolate data obtained from accelerated aging test to real life conditions, aging models are required. So far simple model approaches for lifetime predictions have been reported in literature, like e.g. approaches based on neuronal networks [1]. These approaches usually lack the ability to make extrapolations to conditions that were not used in the learning test set. This work aims to a more physically based approach, able to extrapolate the data from accelerated aging tests to get real life condition lifetime predictions.

Aging in lithium-ion batteries leads to increase of inner resistance, capacity and power loss as well as to changes in impedance spectra due to electrochemical and mechanical processes. Aging strongly depends on temperature, SOC or rather electrode potential, cycling depth and charge throughput [2-4]. Few studies are reported in literature, investigating the calendar and cycle life of different cells using large test matrixes [4-7]. These studies illuminate the aging characteristics of lithium-ion batteries. But so far, this knowledge has not been utilized to develop an aging model that is able to predict the lifetime cycle of real application. Aging models based on mathematical functions obtained from extended aging tests can be directly linked to impedance-based models,

which determine electrical and thermal behavior of the battery [8, 9]. Coupling of impedance-based thermo-electrical battery models with aging models enables investigation of the dynamical interaction between thermal, electrical and aging behavior of the battery. A higher temperature for example causes a faster aging and therefore a faster increase in the inner resistance, affecting the electrical performance of the battery. These relations have been investigated in [10] but lacking a profound parameterization of the developed model using aging test results. This work will focus on the parameterization of the aging model by experimental data using extended aging test results.

2. Experimental

To parameterize impedance-based aging models, extensive aging tests are necessary. In this work a lithium-ion high power pouch cell with a nominal capacity of 6 Ah and a nominal voltage of 3.6 V was used. The anode consists of hard carbon, the cathode of $LiNi_{1/3}Mn_{1/3}Co_{1/3}O_2$ (NMC) as active material. Cells with similar characteristics are typically used in HEV applications.

Extended accelerated calendar aging tests have been performed by storing batteries at constant voltage at different temperatures and different SOC. The test matrix is shown in Table 1. Three cells have been tested under the same condition in order to get statistic relevance. At regular intervals of 6 weeks capacity tests, measurements of the inner resistance of the battery and electrochemical impedance spectroscopy (EIS) were performed at room temperature. Some cells were stored at float conditions (constant voltage), whereas for other cells storage conditions were applied (open circuits). The cells stored with open circuits showed self-discharge processes over time. Therefore, the average voltage during the 6 weeks of storage is used for evaluation of the data. In general, aging tests performed at float conditions are more desirable for the parameterization of aging models, as they ensure constant conditions.

The capacity was determined by a 1C discharge following a standard charge of the cell. For calculation of the inner resistance a high pulse power characterization profile as defined by VDA (German association of the automotive industry) [11] at different depths of discharge was used. Therefore a 18s 4 C-rate discharge pulse followed by a 40 s rest period and a 10s 3 C-rate charge pulse also followed by a 40 s rest period was employed. In this work the so called overall discharge resistance at 20 % DOD calculated by the ratio of voltage change and current during the 40 s rest period after the 4 C-rate discharge pulse is used for the aging analysis.

T / SOC	20 % (3,05 V)	50% (3,51 V)	80 % (3,92 V)	100 % (4,10 V)
25 °C			X	
35 °C	X	X		X
50 °C	X	X	X	X
65 °C		X		X

Table 1: Test matrix of calendar aging tests performed on 6Ah high power lithium-ion batteries with NMC as cathode material.

Impedance spectra were measured at room temperature at different DOD (0%, 20%, 50%, 80%) in galvanostatic mode using frequency range from 5 kHz to 10 mHz. All spectra were measured without superposed DC current at 23°C.

3. Calendar Aging Results

In order to develop and parameterize an aging model, the calendar aging tests were evaluated. In this section the most important results of the aging data are discussed and summarized in order to support the assumptions made for the setup of the model.

It is widely known from literature, that electrolyte decomposition and the corresponding formation of solid electrolyte interphase (SEI), is the dominant aging process in most graphite-based lithium-ion batteries during storage leading to capacity decline (due to loss of active lithium) and impedance rise (due to increase in film layer thickness) [3, 12-14]. Theoretical derivations of the time dependency of the SEI growth rate are quite opposing. Broussely et al. [3] for example describe a formation process taking place at the SEI/electrolyte interface, leading to the conclusion, that the electronic conductivity of SEI is the rate limiting step of formation. Ploehn et al [12] in contrast state a SEI formation that takes place at the anode/SEI interface and is limited by solvent diffusion process. Nevertheless all theories lead to the conclusion that the formation process evolves with a square root of time dependency. A similar trend can be seen in the aging behavior of capacity loss

and internal resistance growth characteristics measured in this work for different storage conditions. Figure 1a shows the actual capacity and Figure 1b the inner discharge resistance over time for cells stored at 50% SOC and different temperatures. In section 5 it will be shown, that the square root of time dependency indeed gives the best fitting result in comparison to various other fitting functions describing the time evolution of the experimental aging data. The spike in the resistance and capacitance after 30 weeks (Figure 1) is due to a measurement error, where the cells were not well connected.

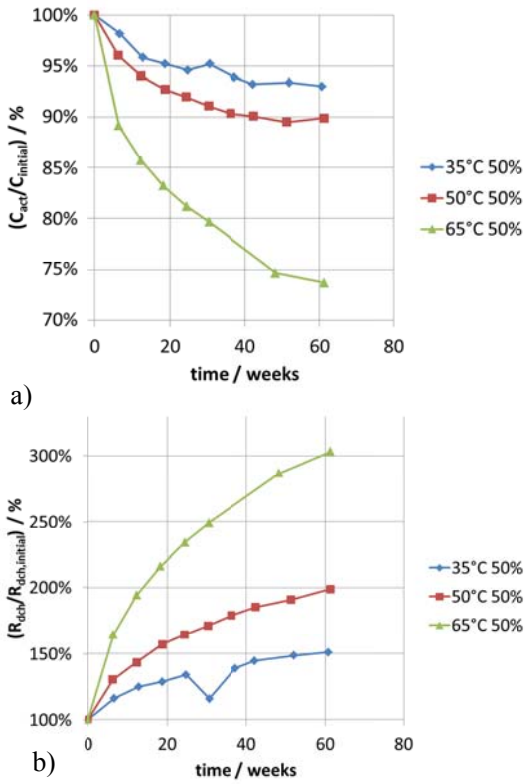

Figure 1: Capacity normalized to initial value (a) and inner resistance normalized to initial value over time is shown for cells stored at 50% SOC and different temperatures. Mean values of three cells stored at the same conditions are displayed.

Figure 2 shows the influence of storage voltage (Figure 2a) and storage temperature (Figure 2b) on aging. The logarithm of capacity fade to basis 2 is plotted over voltage and over invers of temperature, respectively. In both graphs linear tendencies can be observed. Therefore it can be concluded, that capacity fade depends on voltage and temperature in an exponential way. Similar aging behavior was also observed regarding the internal resistance of the cell. This result is in good accordance with Arrhenius law, describing the exponential dependency of reaction rate on temperature. As aging effects during storage are only due to parasitic side reactions, Arrhenius law can be applied here. The voltage dependency in contrast can be quite different, depending on the electrode material used in the cell and the corresponding phase transitions, during intercalation. Depending on the existing phases and phase changes during cycling, the material can show different aging behavior. In some cases of NMC based batteries even a minimum of aging rate could be measured e.g. at SOC around 80%. In $LiMn_2O_4$ Materials also Mn dissolution can lead to an increase of aging at lower SOC [15]. Also the electrolyte and additives account for the voltage range where electrolyte decomposition is favored. Therefore, depending on the cell more detailed investigation of the impact of voltage can be necessary in order to understand its influence.

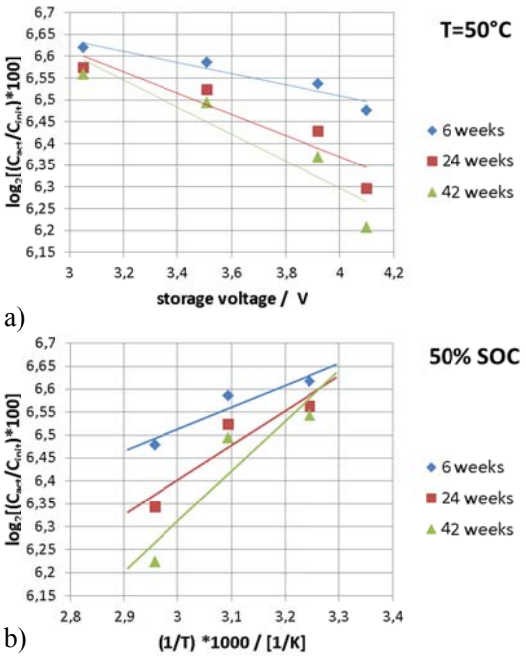

Figure 2: a) normalized capacity fade in a logarithmic scaling to basis 2 over storage voltage for different state of health. The cell was stored at 50°C. b) normalized capacity fade in a logarithmic scaling to basis 2 over the invers temperature for different state of health. The cell was stored at 50% SOC. The mean values of the three cells tested are shown here.

Similar to capacity fade and resistance increase, the obtained impedance spectra were evaluated according to aging dependencies on storage time, temperature and voltage. Figure 3a shows the

evolution of impedance spectra during aging for a cell stored at 65°C and 50% SOC. It can be seen, that especially the intercept with the real axis, usually related to ohmic resistances like resistance of current collector and electrolyte is increasing with proceeding aging. Additionally the mid-frequency semi-circle is enlarging, accounting for the increase of SEI resistance, charge transfer resistance and changes in the behavior of double layer capacity. To evaluate these tendencies in detail, an electric circuit network, shown in Figure 3b, consisting of an inductance, a serial resistance and two ZARC-elements, was used to describe the impedance spectra. The ZARC-element consists of a resistance and a constant phase element in parallel, described by the parameters R, C and Φ [16, 17]:

$$\underline{Z}_{\mathrm{ZARC}} = \frac{R}{1 + R\,C(\mathrm{j}\omega)^{\Phi}}, \qquad \Phi \in [0,1] \tag{1}$$

The inductance describes the inductive part of the spectra, the serial resistance the intercept with the real axis, the first ZARC-element accounts for the mid-frequency semi-circle and the second ZARC-element was used to describe the diffusion behavior.

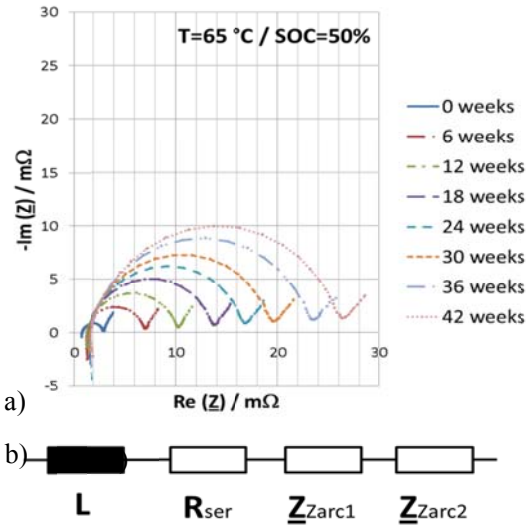

Figure 3: a) Impedance spectra of a cell stored at 65°C and 50% SOC at different state of health. The impedance spectra were measured at 23°C and 80% SOC. b) electric circuit network that was used to evaluate the impedance spectra.

Figure 4a shows the time evolution of the impedance parameters R_{ser}, R_1 and C_1. The sensitivity of the Impedance parameters L, φ_1 and the parameters of the second ZARC-element on aging is small and the data reveal a large scattering over time. Therefore no further investigation has been conducted. The parameter R_1 increases faster in comparison to R_{ser} leading to the conclusion, that SEI formation is the dominant aging process in the cell. Similar to the large signal measurement results, the impedance parameter show a square root of time dependency over lifecycle. Also the temperature and voltage dependency of impedance parameters on aging reveal an exponential dependency, as expected from the theory of SEI formation. The only deviation from exponential behavior was found for the voltage dependency of the impedance parameter R_{ser}. Figure 4b shows a more parabolic dependency of R_{ser} on voltage, which can be related to corrosion of current collector, increasing the ohmic resistance at low SOC, or aging of the electrolyte. Therefore a parabolic function is used to fit the voltage dependency of R_{ser} to the aging data in the following.

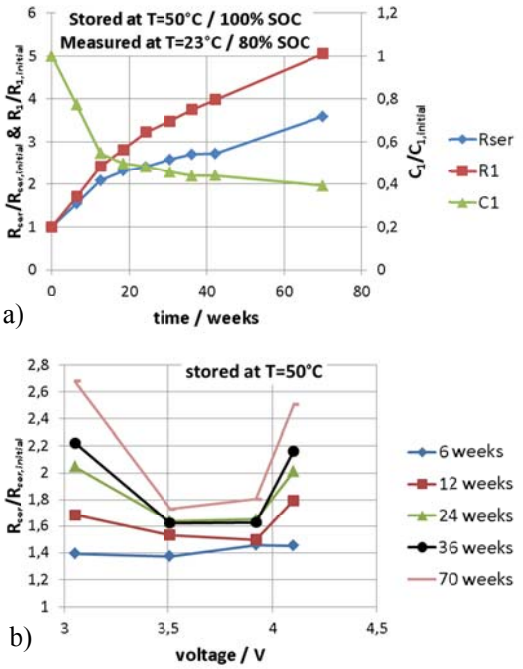

Figure 4: a) shows the impedance parameters R_{ser}, R_1 and C_1 normalized to initial values over time for cells stored at 50°C and 100% SOC. b) shows R_{ser} normalized to initial value over storage voltage for different states of health. The impedance spectra were measured at 23°C and 80% SOC.

Figure 5 shows the evolution of the OCV curve over aging for cells stored at 50°C and 50% SOC. In Figure 5a the OCV over DOD normalized to nominal capacity and in Figure 5b the OCV over DOD normalized to actual capacity is shown. Using the DOD normalized to nominal capacity, the OCV curve changes over aging. Using the DOD normalized to actual capacity in contrast, the OCV curve stays the same. For the use in an aging model, this means, that it is not necessary to change the OCV curve according to the state of health of the battery, but to simply use the latter definition of DOD in order to adjust the OCV.

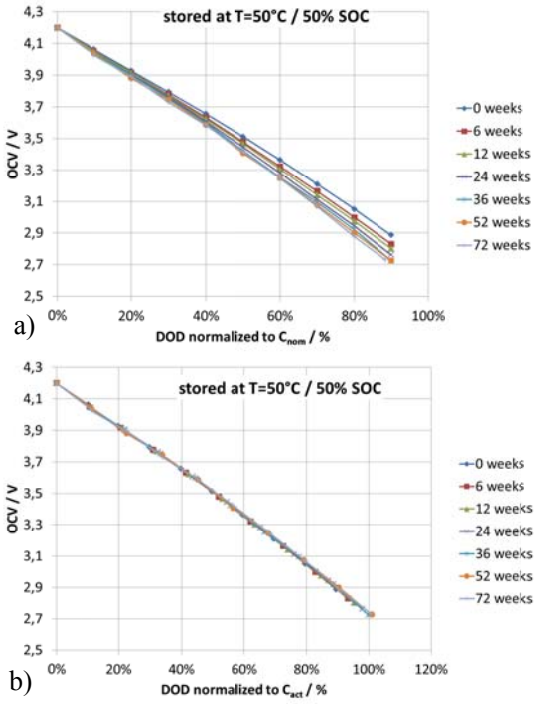

Figure 5: OCV curves over aging for cells stored at 50°C and 50% SOC are shown at different states of health. a) shows the OCV over DOD normalized to nominal capacity and b) the OCV over DOD normalized to actual capacity.

4. Mathematical Description of Aging Behavior

Based on the considerations of the previous section, a lifetime model following a semi-empirical approach can be developed. It has been shown in the extended aging tests, that the following simplifications and assumptions can be used:

- As the cycle life of the batteries exceeds by far the requirements of application in HEV, cycle aging is neglected in the following. Cycle tests where cells were cycled between 60% and 80% SOC have shown, that 30 000 equivalent full cycles can be obtained until the end of capacity life (C_{act} = 70% C_{BOL}) is reached.
- Different resistances evolve in a similar way over aging. Therefore, the total discharge resistance was chosen for the parameterization of the aging model.
- The calendar aging of the cells evolves with a square root of time dependency. This can be seen in fitting results using various fitting functions to describe the time evolution of the experimental aging data (see Table 1).
- The rate of calendar degradation accelerates exponentially with temperature and voltage. Only for the voltage dependency of R_{ser} a parabolic dependency on voltage is used to fit the aging data.
- The aging behavior of the OCV curve can be accounted for, using the actual instead of the nominal capacity for the definition of DOD.
- As the sensitivity of the Impedance parameters L, R_2, C_2, Φ_1 and Φ_2 on aging is small and the data reveal no significant correlation over time, they are taken to be constant over time.

Based on these assumptions the following equations can be derived to fit the measured calendaric aging data:

$$LL_{cal}(t,T,V) = LL_{cal}(t_0,T,V) \cdot \left[1 + A(T,V) \cdot F(t)\right] \quad , \qquad (2)$$

where LL_{cal} is used for the evolution of capacity, inner resistance or impedance parameters either. $F(t)$ describes the time dependency and is related to the dominant aging processes or their combination:

$$F(t) = c_a \cdot t^{\beta} \quad . \qquad (3)$$

c_a is a coefficient describing the rate of aging at reference conditions T_0 and V_0 depending on the specific process. Under the assumption of electrolyte decomposition being the dominant aging process, β becomes 0.5.

$A(T,V)$ describes the impact of temperature and potential on the calendar degradation rate according to:

$$A(T,V) = c_T^{\frac{T-T_0}{\Delta T}} \cdot c_V^{\frac{V-V_0}{\Delta V}} \qquad (4)$$

The first factor describes the temperature impact on the aging rate, the second one the impact of the potential. c_T and c_V are fitting parameters, describing the impact of temperature and voltage on aging, respectively. T_0 and V_0 are reference temperature and voltage and can be chosen arbitrarily. For the following we chose T = 25°C and V_0 = 3.5V. ΔT was set to 10°C, meaning, that an increase in temperature by 10°C results in an increase in aging by a factor c_T compared to reference conditions T_0. Similarly ΔV was set to 0.1V. Similar equations have been also used by Bohlen et al. [8, 9] to describe the aging behavior of super capacitors.

The only exception has been found in the aging evolution of the impedance parameter R_{ser}, where a parabolic dependency on voltage has been detected (see Figure 4b). Therefore to describe the aging evolution of R_{ser} eq. (4) was substituted by:

$$A(T,U) = c_T^{\frac{T-T_0}{\Delta T}} \cdot \left(c_V \cdot \left(\frac{V-V_0}{\Delta V} \right)^2 + 1 \right) \qquad (5)$$

Eq. (2) was used to fit the extended aging data, leaving the parameters c_a, c_T and c_V free for regression analysis. Non-linear least square algorithm was used for regression. The fits include data of the test matrix, introduced in section 3, containing about 30 batteries stored at different temperatures and voltages. For comparison, beside square root of time dependencies also combinations of square root of time and linear time dependencies as well as combinations of square root of time and logarithmic time dependencies have been investigated in fittings. To assess the goodness of fit an analysis of correlation coefficient R^2 was carried out. Table 1 compares the fit results of the different approaches for the capacity fade. Especially considering the linear behavior, it can be seen, that the linear contribution to the fit is very small or even zero. Therefore apart from increasing the number of free parameters the linear term did not yield significant improvement compared to eq. (2). The fitting results for the functions including a logarithmic term show, that also logarithmic time dependency can be an approach to describe calendar aging. The difference to the square root dependency is that the logarithmic time dependency is steeper in the beginning and becomes flatter later. Therefore it overestimates the aging at the beginning, but yields better results after some time. As the logarithmic behavior lacks of physical explanation, we will focus on the square root dependency in the following. Square root function on time can be directly derived from theoretical investigation of SEI formation. The physical process behind the mathematical expression is the critical issue to ensure the ability of the model for extrapolations.

In Table 2 the values of the resulting fitting parameters for capacity fade, resistance increase and impedance parameters using eq. (2) and the corresponding correlation coefficients R^2 are shown. The parameters describing the capacity evolution indicate an acceleration of aging by a factor of c_T = 1.55 caused by a temperature increase of ΔT= 10°C compared to T_0. For potential dependency of the capacity, fitting reveals an acceleration factor of c_V = 1.15 for an increase of ΔV = 0.1 V. This differs from the rule of thumb, predicting that aging rate doubles by increasing the temperature by 10°C or the voltage by 0.1 V. The aging rate at reference conditions T_0 and U_0 becomes c_a = 0.0064. Similar results are received for the inner resistance and the impedance parameters R_{ser}, R_1, C_1, differing slightly as they are impacted by different aging effects. Thus this approach convinces due to its simplicity and its physical correspondent.

Equation	Parameter	Parameter value	R^2	Number of free parameter
$\frac{C(t)}{C_{init}} = 1 + c_a \cdot c_V^{\frac{V-V_0}{\Delta V}} \cdot c_T^{\frac{T-T_0}{\Delta T}} \cdot \sqrt{t}$	c_a	-0,0064	0,9341	3
	c_V	1,1484		
	c_T	1,5479		
$\frac{C(t)}{C_{init}} = 1 + c_V^{\frac{V-V_0}{\Delta V}} \cdot c_T^{\frac{T-T_0}{\Delta T}} \left[c_{a1} \cdot \sqrt{t} + c_{a2} \cdot t \right]$	c_{a1}	-0,0064	0,9341	4
	c_{a2}	0		
	c_V	1,1484		
	c_T	1,5479		
$\frac{C(t)}{C_{init}} = 1 + c_{a1} \cdot c_{V1}^{\frac{V-V_0}{\Delta V}} \cdot c_{T1}^{\frac{T-T_0}{\Delta T}} \cdot \sqrt{t} + c_{a2} \cdot c_{V2}^{\frac{V-V_0}{\Delta V}} \cdot c_{T2}^{\frac{T-T_0}{\Delta T}} \cdot t$	c_{a1}	-0,0053	0,9447	6
	c_{V1}	1,1392		
	c_{T1}	1,6389		
	c_{a2}	-0,00005		
	c_{V2}	1,87333		
	c_{T2}	0,59485		
$\frac{C(t)}{C_{init}} = 1 + c_a \cdot c_V^{\frac{V-V_0}{\Delta V}} \cdot c_T^{\frac{T-T_0}{\Delta T}} \cdot \log t$	c_a	-0,010392	0,9365	3
	c_V	1,15069		
	c_T	1,554253		
$\frac{C(t)}{C_{init}} = 1 + c_V^{\frac{V-V_0}{\Delta V}} \cdot c_T^{\frac{T-T_0}{\Delta T}} \left[c_{a1} \cdot \sqrt{t} + c_{a2} \cdot \log t \right]$	c_{a1}	-0,00291	0,9433	4
	c_{a2}	-0,00565		
	c_V	1,14959		
	c_T	1,55187		
$\frac{C(t)}{C_{init}} = 1 + c_{a1} \cdot c_{V1}^{\frac{V-V_0}{\Delta V}} \cdot c_{T1}^{\frac{T-T_0}{\Delta T}} \cdot \sqrt{t} + c_{a2} \cdot c_{V2}^{\frac{V-V_0}{\Delta V}} \cdot c_{T2}^{\frac{T-T_0}{\Delta T}} \cdot \log t$	c_{a1}	-0,00094	0,9604	6
	c_{V1}	1,055624		
	c_{T1}	2,255951		
	c_{a2}	-0,008921		
	c_{V2}	1,225323		
	c_{T2}	1,284523		

Table 1: Fit results for different mathematical functionalities for the capacity fade are shown.

	c_a	c_V	c_T	R^2
Capacity	-0.0064	1.1484	1.5479	0.934
Resistance	0.0484	1.0670	1.5665	0.96
R_{ser}	0.0206	0.0471	1.7586	0. 85
R_1	0.0766	1.0618	2.1437	0.89
C_1	-0.0457	1.0258	1.2248	0.79

Table 2: Fitting parameters for capacity fade, resistance increase and impedance parameters R_{ser}, R_1 and C_1 using eq. (2) and the corresponding correlation coefficients R^2

Fitting results for the evolution of capacity and overall resistance during storage at 50% SOC at different temperatures are shown exemplarily in Figure 6. The fittings for these values yield good results, with a R^2 of 0.934 and 0.96, respectively. It has to be kept in mind that data of about 30 cells at a variety of storage conditions have been fitted using one set of parameters. This of course yields deviations of the fit from the data at certain conditions. Nevertheless the overall fitting result is unquestionable.

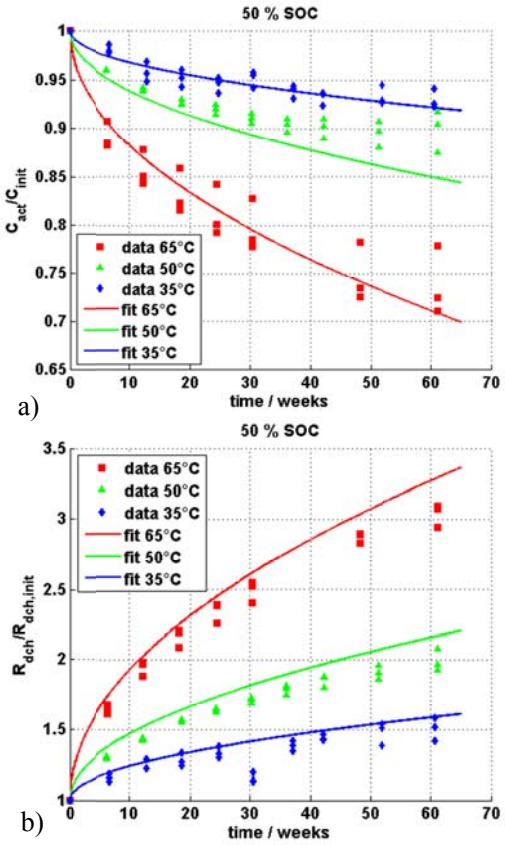

Figure 6: Fitting results for a) capacity fade (actual capacity normalised to initial capacity) and b) resistance increase (actual resistance normalised to initial resistance) over time using eq. (2) is shown for cells stored at 50% SOC at different temperatures. The dots mark the measured data results for the cells, the lines the fittings.

Equation (2) also yields good results for the description of the fittings of the Impedance parameters. For R_{ser} a parabolic voltage dependency was taken into account. Even though the data concerning impedance parameters are scattering more compared to the capacity and resistance data, correlation coefficients between 0.79 and 0.89 could be obtained. The scattering in the data is due to the additional fitting step to determine impedance parameters using the electric circuit diagram in Figure 3b. The fitting results for the evolution of the impedance parameters R_{ser}, R_1 and C_1 for cells stored at 50% SOC at different temperatures are shown in Figure 7.

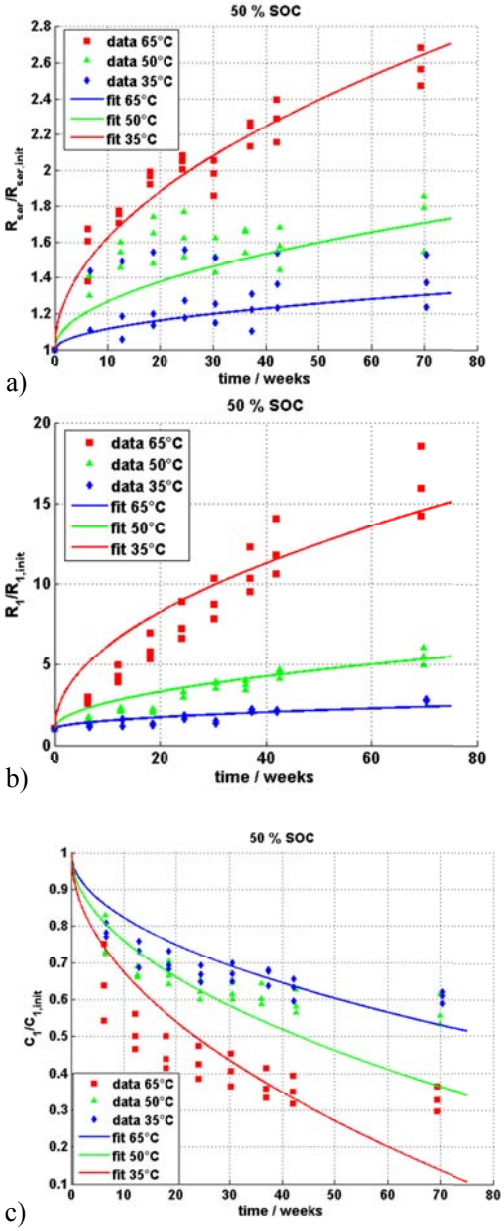

Figure 7: Fitting results for the evolution of the impedance parameters a) R_{ser}, b) R_1 and c) C_1 using eq. (2) for cells stored at 50% SOC at different temperatures are shown. The values are normalized to the initial value. The dots mark the measured data results for the cells, the lines the fittings.

5. Development of Lifetime Model

The fitting results of the calendar aging data can be used to develop a model to predict lifetimes under different operation conditions by combining an impedance-based electro-thermal model with the mathematical expressions obtained from the test results. Such a semi-empirical model approach for lifetime predictions has the advantage of an easy parameterization based on accelerated calendar

lifetime tests and an acceptable computing time. Moreover the approach enables extrapolations to different operation conditions, e.g. to lower temperature, as the mathematical equations derived in section 4 are based on physical aging processes in the battery. This is an advantage of such a model approach in comparison to e.g. models using neuronal network approaches that are restricted to the conditions of the aging data used as learning set. It is therefore an important goal of the semi-empirical approach to derive a set of empirical equations for the aging, using mathematical expressions that are close to the main degradation mechanisms.

The electrical model used in this work is an impedance-based model, using the electric circuit diagram in Figure 3b with an additional serial capacity C_d to describe the impedance spectra at different temperatures and voltages. The resulting impedance parameters are given to the model as lookup tables for different temperatures and voltages. To parameterize the current dependency of the impedance parameters, the current dependency of the inner resistance obtained from pulse power profiles was used. The electrical network is then used in the model to calculate the voltage response of the cell to a current pulse. The thermal model is based on a simple thermal network including an ohmic heat production as a one point source, a heat capacity and thermal conductivity in each direction in space to simulate heat transfer with the environment. More details on the model can be found in [18], where also the validation of the model for the cell used in this work can be found. The thermal, as well as the dynamic electrical behavior can be simulated accurately. A similar approach was also used in [16, 19]

As aging depends strongly on temperature and voltage, the aging model receives temperature and voltage evolution calculated by the thermo-electrical model. In each time step, the infinitesimal aging of the cell due to the predominating conditions, i.e. temperature and voltage, is calculated. Depending on the application and on the applied current profile, temperature and voltage vary over time. Therefore it is necessary to add up the incremental loss of life time in the model using equation (2):

$$LL_{cal}(t,T(t),V(t)) = LL_{cal}(t_0,T(t_0),V(t_0)) + \sum_{i=1}^{N} \frac{dLL_{cal}(LL_{cal}(t_{i-1}),T(t_i),V(t_i))}{dt_i}\Delta t_i \quad (6)$$

Finally all parameters of the electrical model, like capacity, inner resistance and impedance parameters are updated according to their actual state of health following eq. (6) in each time step. It is important to note that we assumed the actual degradation, e.g. capacity fade and resistance to be dominated by SEI growth. As the rate of SEI growth is mainly determined by the layer thickness, capacity fade and resistance increase are directly proportional to the change in layer thickness. Since not the ongoing time, but the layer thickness is the only continuous parameter during varying temperature and voltage, the time has to be substituted by the actual capacity or resistance in eq. (6), representing SEI thickness. Figure 8 shows schematically the working principle of the model.

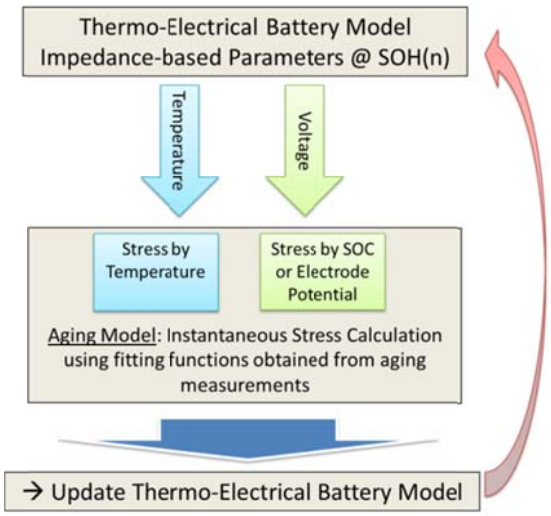

Figure 8: Working principle of the semi-empirical aging model.

6. Simulation Results

For the simulation of the cell a realistic current profile for HEV according to VDA was used to cycle the battery and to investigate the aging under realistic operation conditions. The current rates have been adjusted according to the cell specifications. Using the profile shown in Figure 9 the batteries were cycled at 40°C between 60%-80%, 45%-65% and 30%-50% SOC.

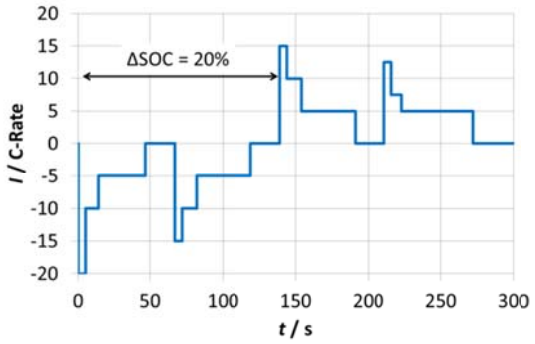

Figure 9: HEV profile applied for the simulations.

Figure 10 shows the capacity fade and resistance increase during cycling of the cell with the HEV profile. Wheras end of capacity life (80% of initial capacity) is already reached after about 2 years while cycling the battery between 60%-80% SOC, even 6 years of lifetime can be obtained, when the battery is cycled only between 30%-50% SOC. The higher state of charge leads to a faster degradation. It can also be seen that the end of resistive life (initial resistance doubles) is reached much faster compared to end of capacity life.

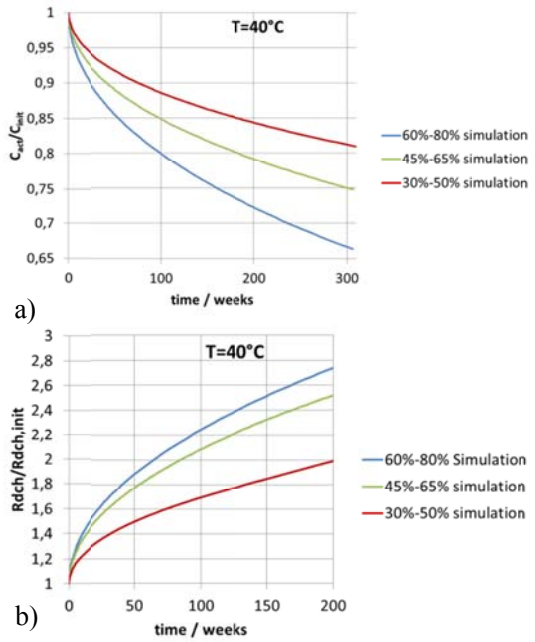

Figure 10: Simulation results for a) capacity fade (actual capacity normalised to initial capacity) and b) resistance increase (actual resistance normalised to initial resistance) over time is shown, for the cell cycled at 40 °C with the HEV profile between different SOC.

7. Conclusions

In this work a simulation model was presented to predict lifetime of a lithium-ion battery under realistic operation condition. The model approach couples an impedance based electric-thermal model to a semi-empirical aging model, to account for the impact of aging on the dynamical behavior of the battery. The aging model is based on results obtained from extended accelerated aging tests, which were used to parameterize the model. From the aging test results simplifications for the model approach could be derived. It was observed that calendar aging test results can be used for a first approximation of lifetime, as cycle life of the batteries exceeds by far the requirements of application. Test results showed, that a square root of time dependency can be applied to the data, as well as an exponential behavior of aging on voltage and temperature. The aging behavior of the OCV curve was accounted for, using the actual instead of the nominal capacity for the definition of DOD. The sensitivity of the Impedance parameters L, R_2, C_2, Φ_1 and Φ_2 on aging is small and was therefore neglected. Mathematical functions, based on physical aging effects, were obtained from the test results to describe the aging behavior and to ensure the ability of the model to make extrapolations. The functions were implemented in a semi-empirical aging model. Based on the model different drive cycles, use patterns and management strategies can be analyzed with regard to their impact on lifetime. Exemplarily the impact of a realistic HEV profile on the aging of a high power cell was simulated for different operation ranges. More detailed accounts on the results as well as a verification of the model are presented in a paper submitted to the Journal of Power Sources.

Acknowledgment

This work has been done in the framework of the research initiative “KVN” funded by the German Federal Ministry for Education and Research, funding number 13N9973. Responsibility for the content of this publication lies with the author.

References

[1] R. G Jungst, G. Nagasubramanian, H. L Case, B.Y.Liaw, A. Urbina, T. L Paez, D. H Doughty *Accelerated calendar and pulse life analysis of lithium-ion cells*, J. Power Sources 119–121 (2003), 870-873

[2] J. Vetter, P. Novák, R. M. Wagner, C. Veit, K.-C. Möller, J. O. Besenhard, M. Winter, M. Wohlfahrt-Mehrens, C. Vogler, A. Hammouche. *Ageing mechanisms in lithium-ion batteries*, J. Power Sources 147 (2005), 269 – 281

[3] M. Broussely, S. Herreyre, P. Biensan, P. Kasztejna, K. Nechev, R. J. Staniewicz. *Aging mechanism in Li ion cells and calendar life predictions*, J. Power Sources 97-98 (2001), 13-21

[4] M. Broussely, P. Biensan, F. Bonhomme, P. Blanchard, S. Herreyre, K. Nechev, R. J. Staniewicz. *Main aging mechanisms in Li ion batteries*, J. Power Sources 146 (2005), 90-96

[5] R.B Wright, C.G Motloch, J.R Belt, J.P Christophersen, C.D Ho, R.A Richardson, I Bloom, S.A Jones, V.S Battaglia, G.L Henriksen, T Unkelhaeuser, D Ingersoll, H.L Case, S.A Rogers, R.A Sutula, *Calendar- and cycle-life studies of advanced technology development program generation 1 lithium-ion batteries*, J. Power Sources 110 (2002), 445-470

[6] I. Bloom, S. A. Jones, E. G. Polzin, V. S. Battaglia, G. L. Henriksen, C. G. Motloch, R. B. Wright, R. G. Jungst, H. L. Case, D. H. Doughty, *Mechanisms of impedance rise in high-power, lithium-ion cells*, J. Power Sources 111 (2002), 152-159

[7] J. Wang, P. Liu, J. Hicks-Garner, E. Sherman, S. Soukiazian, M. Verbrugge, H. Tataria, J. Musser, P. Finamore, *Cycle-life model for graphite-LiFePO$_4$ cells, J. Power Sources 196 (2011), 3942-3948*

[8] O. Bohlen, J. Kowal, D. U. Sauer, *Ageing behaviour of electrochemical double layer capacitors Part I. Experimental study and ageing model,* Journal of Power Sources 172 (2007) 468–475

[9] O. Bohlen, J. Kowal, D. U. Sauer, *Ageing behaviour of electrochemical double layer capacitors Part II. Lifetime simulation model for dynamic application,* Journal of Power Sources 173 (2007) 626–632

[10] J. B. Gerschler, H. Witzenhausen, F. Hust, D. U. Sauer, *Three-Dimensional Performance and Lifetime Model for Lithium-Ion Batteries – Spatially-Resolved Models are Required for Accurate Simulation of Large-Sized Cells*, Electric Vehicle Symposium (EVS-25) Shenzhen, China, Nov. 5-9, 2010

[11] *Test Specification for Li-Ion Battery Systems for Hybrid Electric Vehicles*, Association of the German automotive industry (VDA), Release 1.0, 2007

[12] H. J. Ploehn, P. Ramadass, R. E. White, *Solvent Diffusion Model for Aging of Lithium-Ion Battery Cells*, J. Electrochem. Soc. 151, A456 (2004)

[13] D. Aurbach, *Review of selected electrode–solution interactions which determine the performance of Li and Li ion batteries,* J. Power Sources 89 (2000), 206-218

[14] R. Spotnitz, *Simulation of capacity fade in lithium-ion batteries, J. Power Sources 113 (2003*), *72-80*

[15] Y. Nishi, *Lithium ion secondary batteries; past 10 years and the future, J. Power Sources 100 (2001), 101-106*

[16] S. Buller, M. Thele, K. Kahlen, R. W. De Doncker, *Impedance-based simulation models of supercapacitors and Li-ion batteries for power electronic applications,* IEEE TRANSACTIONS ON INDUSTRY APPLICATIONS (2005), 41(3), 742-747

[17] S. Buller, *Impedance-based simulation models for energy storage devices in advanced automotive power systems,* Dissertation, RWTH Aachen, Shaker Verlag, 2003, ISBN 3-8322-1225-6

[18] S. Käbitz, D. U. Sauer, *Impedance spectroscopy to model lithium-ion batteries*, International Workshop on Impedance Spectroscopy, October 2011, Chemnitz, Germany

[19] D. Andre, M. Meiler, K. Steiner, H. Walz, T. Soczka-Guth, D.U. Sauer, *Characterization of high-power lithium-ion batteries by electrochemical impedance spectroscopy. II: Modelling,* J. Power Sources, 196 (2011) 5349-5356

Authors

Dipl.-Phys. Madeleine Ecker
Institute for Power Electronics and Electrical Drives (ISEA), RWTH Aachen University
Jaegerstrasse 17 – 19, D-52066 Aachen
Tel: +49-241-8096977
Fax: +49-241-8092203
Email: er@isea.rwth-aachen.de
URL: www.isea.rwth-aachen.de

Madeleine Ecker received his diploma in Physics from University of Heidelberg in 2009. In July 2009 she joined ISEA as a research associate. Since October 2010 she is team leader for ISEA's activities in the field of modeling. Her areas of interest are empirical as well as physico-chemical modeling of lithium-ion batteries with a special focus on cell ageing.

Dipl.-Ing. Jochen Bernhard Gerschler
Institute for Power Electronics and Electrical Drives (ISEA), RWTH Aachen University, Email: ge@isea.rwth-aachen.de

Jochen Bernhard Gerschler received his diploma degree from Technical University of Dortmund in 2005. He worked at ISEA as a research associate from July 2005 till March 2011. Since September 2009 until he left ISEA he was team leader for ISEA's activities in the field of lithium-ion batteries. His areas of interest are modeling and characterization of Li-Ion and NiMH batteries with a special focus on spatially resolved modeling and cell aging.

BSc. JanVogel
Institute for Power Electronics and Electrical Drives (ISEA), RWTH Aachen University, Email: jan.vogel@rwth-aachen.de

Jan Vogel studies Electrical Engineering at the RWTH Aachen University. He did his bachelor thesis at ISEA about aging mechanisms in lithium-ion batteries.

Dipl.-Ing. Stefan Käbitz
Institute for Power Electronics and Electrical Drives (ISEA), RWTH Aachen University, Email: kb@isea.rwth-aachen.de

Stefan Käbitz received his diploma degree from the RWTH Aachen University in 2010. In March 2010 he joined ISEA as research associate. Since April 2011 he is team leader for ISEA´s activities in the field of lithium-ion batteries. His areas of interest are impedance-based as well as physico-chemical models for lithium-ion batteries with a special focus on EIS.

Cand. Wirt.-Ing. Friedrich Hust
Institute for Power Electronics and Electrical Drives (ISEA), RWTH Aachen University, Email: friedrich.hust@isea.rwth-aachen.de

Friedrich Hust studies industrial engineering with his major in Electrical Power Engineering at the RWTH Aachen University. Since 2008 he has been working as a student assistant at the ISEA. He expects to finish his Dipl.Wirt.-Ing degree in 2012.

Cand. B. Sc. Philipp Dechent
Institute for Power Electronics and Electrical Drives (ISEA), RWTH Aachen University, Email: philipp.dechent@isea.rwth-aachen.de

Philipp Dechen studies Electrical Engineering at the RWTH Aachen University. Since 2010 he has been working as a student assistant at the ISEA. He expects to finish his bachelor degree in 2012.

Univ.-Prof. Dr. rer. nat. Dirk Uwe Sauer
Institute for Power Electronics and Electrical Drives (ISEA), RWTH Aachen University
Email: sr@isea.rwth-aachen.de

Dirk Uwe Sauer received his diploma in Physics from University of Darmstadt in 1994. From 1994 -2003 he worked at Fraunhofer ISE as a research scientist, from 2000 – 2003 as team leader for "Storage Systems". After receiving his PhD from University of Ulm in 2003, topic: "Optimisation the usage of lead-acid batteries in photovoltaic-hybrid systems with special emphasis on battery aging", he joined ISEA as professor for Electrochemical Energy Conversion and Storage Systems.